EURASIP Journal on Applied Signal Processing 2005:3, 382–396

Principles and Limitations of Ultra-Wideband FM Communications Systems

John F. M. Gerrits
Centre Suisse d'Electronique et de Microtechnique SA, Jaquet-Droz 1, CH-2007 Neuchâtel, Switzerland
Email: john.gerrits@csem.ch

Michiel H. L. Kouwenhoven
National Semiconductor BV, Amplifier Design Europe, Delftech Park 19, 2628 XJ Delft, The Netherlands
Email: michiel.kouwenhoven@nsc.com

Paul R. van der Meer
Electronics Research Laboratory/DIMES, Faculty of Electrical Engineering, Mathematics and Computer Science (EEMCS), Delft University of Technology, Mekelweg 4, 2628 CD Delft, The Netherlands
Email: p.r.vandermeer@ewi.tudelft.nl

John R. Farserotu
Centre Suisse d'Electronique et de Microtechnique SA, Jaquet-Droz 1, CH-2007 Neuchâtel, Switzerland
Email: john.farserotu@csem.ch

John R. Long
Electronics Research Laboratory/DIMES, Faculty of Electrical Engineering, Mathematics and Computer Science (EEMCS), Delft University of Technology, Mekelweg 4, 2628 CD Delft, The Netherlands
Email: j.r.long@ewi.tudelft.nl

Received 10 October 2003; Revised 7 March 2004

This paper presents a novel UWB communications system using double FM: a low-modulation index digital FSK followed by a high-modulation index analog FM to create a constant-envelope UWB signal. FDMA techniques at the subcarrier level are exploited to accommodate multiple users. The system is intended for low (1–10 kbps) and medium (100–1000 kbps) bit rate, and short-range WPAN systems. A wideband delay-line FM demodulator that is not preceded by any limiting amplifier constitutes the key component of the UWBFM receiver. This unusual approach permits multiple users to share the same RF bandwidth. Multipath, however, may limit the useful subcarrier bandwidth to one octave. This paper addresses the performance with AWGN and multipath, the resistance to narrowband interference, as well as the simultaneous detection of multiple FM signals at the same carrier frequency. SPICE and Matlab simulation results illustrate the principles and limitations of this new technology. A hardware demonstrator has been realized and has allowed the confirmation of theory with practical results.

Keywords and phrases: UWB, FM, FDMA, WPAN, subcarrier, multipath.

1. INTRODUCTION

Ultra-wideband (UWB) communications systems are poised to play an increasingly important role in today's short-range communications systems, especially personal area network (PAN) applications. By definition, the −10 dB RF bandwidth B_{RF} of a UWB signal centered at a frequency f_c should be at least 20% of this central frequency or at least 500 MHz for operation above 3.1 GHz [1]. Since the definition of a UWB signal does not specify a particular air interface or modulation scheme, many different techniques may be applicable to a UWB signal.

Originally, UWB started as an impulse radio, using a time-domain approach [2]. Instead of a continuous sinusoidal carrier, a sequence of short-duration pulses is used as the information carrier. The spectrum of such a pulse

sequence (usually Gaussian) has a single broad main lobe with slow spectral roll-off. These pulsed systems were originally intended for radar applications where short pulse duration translates into a high resolution. When used in a communications system, the pulse sequence can be modulated using, for example, pulse-amplitude modulation (PAM) or pulse-position modulation (PPM) techniques.

UWB communications technology was originally intended to provide robust, easy-to-implement, low-cost, and low-power consumption solutions. An impulse radio or multicarrier OFDM system, as proposed recently [3], may be able to provide a robust high data rate solution, but this comes at the expense of circuit complexity and power consumption.

The goal of the authors was to search for a complementary low and medium data rate (LDR and MDR) UWB system that is easy to implement in silicon, provides robustness to interference compared to narrowband ISM solutions, and is competitive in terms of power consumption [4].

The proposed solution is a constant-envelope frequency-domain approach called UWB frequency modulation (UWBFM) [5]. This double FM scheme uses low-modulation index FSK followed by high-modulation index analog FM to achieve the wide bandwidth. Different users distinguish themselves by different subcarrier frequencies. This approach has a number of attractive properties for use in short-range wireless personal area network (WPAN) systems, where the dynamic range of the RF signals is limited.

The paper starts by presenting the principles of UWBFM technology in Section 2. Block diagrams of both the transmitter and the receiver are presented and an example of a multiuser system is given. Section 3 discusses the operation of the wideband FM delay-line demodulator in the presence of a single FM signal. In Section 4, the overall receiver performance under additive white Gaussian noise (AWGN) conditions is examined. The nonlinear relationship between the input and output signal-to-noise ratio (SNR) of the wideband FM demodulator strongly influences the receiver performance. Section 5 presents a multiuser UWBFM system based upon frequency division multiple access (FDMA) subcarrier technology, and shows mathematically why this works. It also addresses the closely related issue of the robustness of UWBFM to narrowband interference. Section 6 addresses the effect of multipath on an UWBFM system. Section 7 presents conclusions and topics for further investigations.

2. PRINCIPLES OF UWBFM

UWBFM can be seen as an analog implementation of a spread-spectrum system with a spreading gain equal to the modulation index β. FM has the unique property that the RF bandwidth B_{RF} is not only related to the bandwidth f_m of the modulating signal, but also to the modulation index β that can be chosen freely. This yields either a bandwidth-efficient narrowband FM signal ($\beta < 1$) or a (ultra-) wideband signal ($\beta \gg 1$) that can occupy any required bandwidth compatible with the RF oscillator's tuning range.

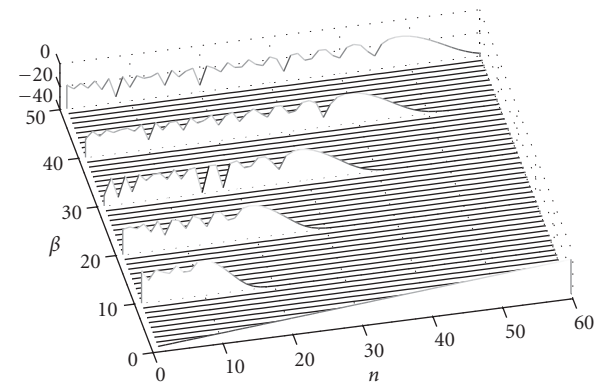

Figure 1: Amplitude of the Bessel functions ($20 \log_{10}(J_n(\beta))$) for various values of the modulation index β.

Assume an FM signal $V(t)$ with amplitude A and carrier frequency f_c ($\omega_c = 2\pi f_c$) modulated by a sinusoidal signal $m(t)$ of frequency $f_m(\omega_m = 2\pi f_m)$ such that

$$m(t) = V_m \sin(\omega_m t). \tag{1}$$

An RF oscillator sensitivity of K_O [rad/Vs] yields a deviation $\Delta\omega = 2\pi\Delta f$ equal to

$$\Delta\omega = K_O V_m, \tag{2}$$

resulting in an FM signal $V(t)$:

$$\begin{aligned} V(t) &= A \sin(\omega_c t + \varphi(t)) \\ &= A \sin\left(\omega_c t + K_O \int_{-\infty}^{t} V_m \sin(\omega_m \tau)\, d\tau\right) \\ &= A \sin\left(\omega_c t - \frac{K_O V_m}{\omega_m} \cos(\omega_m t) + \varphi_0\right) \\ &= A \sin(\omega_c t - \beta \cos(\omega_m t) + \varphi_0), \end{aligned} \tag{3}$$

where $\varphi(t)$ is the instantaneous phase excursion due to the FM, φ_0 is an arbitrary but time-independent constant, and β is the modulation index defined by

$$\beta = \frac{\Delta f}{f_m} = \frac{\Delta\omega}{\omega_m}. \tag{4}$$

Equation (3) can be expressed as a sum of Bessel functions $J_n(\beta)$ of the first kind (order n) of the argument β:

$$V(t) = A \sum_{n=-\infty}^{\infty} J_n(\beta) \sin(\omega_c + n\omega_m)t. \tag{5}$$

Theoretically, the spectrum of an FM signal is infinitely large. In practice, the higher-order Bessel functions $J_n(\beta)$ decay rapidly for $n > \beta$. Figure 1 shows the value of the Bessel functions $J_n(\beta)$ for various values of modulation index β. The bandwidth of an FM signal is well approximated

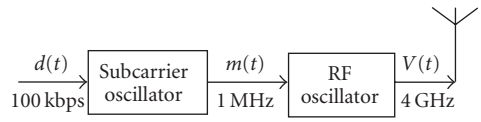

Figure 2: Block diagram of the UWBFM transmitter.

by Carson's rule:

$$B_{\mathrm{RF}} \approx 2(\beta + 1) f_m = 2(\Delta f + f_m). \tag{6}$$

As a result of the fast decay of the Bessel functions for $n > \beta$, the bandwidth of a wideband FM signal can be controlled by adapting the modulation index β. When the modulation index $\beta \gg 1$, a wideband spectrum is obtained in which no carrier can be distinguished. The spectral roll-off of this UWBFM signal is very steep. This strongly improves the coexistence of UWBFM systems with other RF systems operating in adjacent frequency bands. Analog FM can thus be used as a spreading mechanism to generate an unmodulated constant-envelope UWB signal of appropriate bandwidth. An additional modulation mechanism is still required to modulate data upon this UWB signal.

Figure 2 shows the block diagram of the UWBFM transmitter. The additional modulation mechanism is digital FM by a raw data signal $d(t)$ of the low-frequency subcarrier using FSK techniques with modulation index $\beta_{\mathrm{SUB}}(0.5 < \beta_{\mathrm{SUB}} < 4)$.

Individual users are assigned separate subcarrier frequencies. The approximate bandwidth B_{SUB} of a subcarrier modulated by a lowpass filtered digital signal of bit rate R (bps) equals

$$B_{\mathrm{SUB}} = R(\beta_{\mathrm{SUB}} + 1). \tag{7}$$

Figure 3 shows the data, the subcarrier, and the UWB signal in the time domain for a data transition at $t = 0$ and subcarrier frequency of 1 MHz; the center frequency of the UWB signal $V(t)$ was chosen to be 10 MHz for the sake of visibility.

The choice of the subcarrier frequencies $f_{\mathrm{SUB}\,i}$ and modulation indices $\beta_{\mathrm{SUB}\,i}$ is determined by the data rate(s) and the number of users in the UWBFM communications system. A low-subcarrier modulation index yields a lower subcarrier bandwidth allowing more users. On the other hand, it requires steeper subcarrier filtering in the receiver. This is especially true since the wideband FM demodulator has a quadratic transfer function resulting in an expanded subcarrier dynamic range. In the context of a short-range WPAN, this limited dynamic range (typically 30 dB) can be accepted. We will show in Section 6 that when no equalization is used, multipath may limit the useful subcarrier frequency range to one octave.

An example of a hybrid system providing both LDR and MDR subcarriers are shown in Figure 4. The 3 LDR users (1–3) operate at 10 kbps with a modulation index $\beta_{\mathrm{SUB}} = 1$ yielding a bandwidth of 20 kHz. They are spaced 150 kHz apart. The single MDR user (4) operates at 100 kbps and uses a modulation index $\beta_{\mathrm{SUB}} = 2$, yielding a bandwidth of 300 kHz.

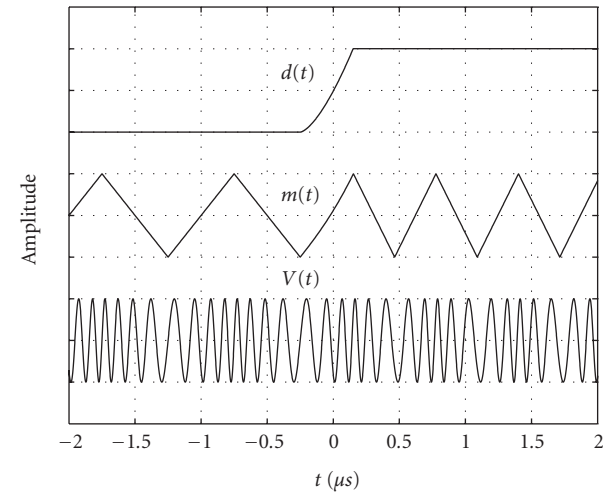

Figure 3: Time-domain view of data $d(t)$, subcarrier $m(t)$, and UWB signal $V(t)$.

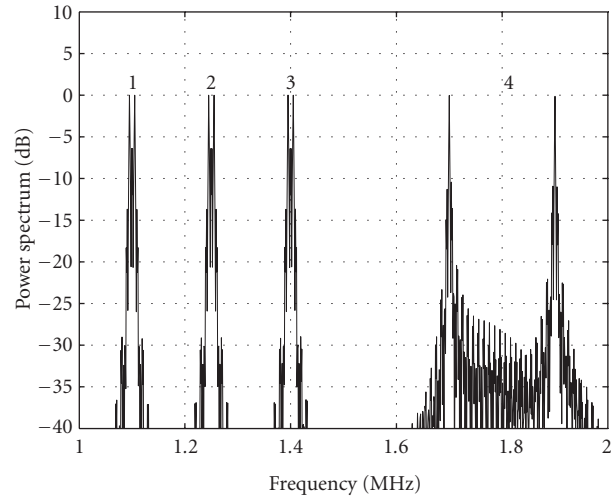

Figure 4: Spectrum $S(f)$ after the wideband FM demodulator in the receiver for a hybrid LDR-MDR 1–2 MHz subcarrier system.

The UWB signal $V(t)$ is obtained by feeding the modulated subcarrier signal $m(t)$ into the FM input of the RF oscillator operating at the desired center frequency (f_c) of the UWB signal.

Figure 5 shows an example of the spectral density of such an UWBFM signal. The signal power is −13 dBm (140 $\mathrm{mV_{p\text{-}p}}$ in a 50Ω load). The subcarrier frequency is 1 MHz and the deviation Δf is 600 MHz, yielding a modulation index β of 600. The −10 dB bandwidth is almost equal to the bandwidth predicted by Carson's rule in (6):

$$B_{-10\,\mathrm{dB}} \approx 2\Delta f. \tag{8}$$

The spectral density is lowered by a factor of $10\log_{10}(\beta) = 28$ dB. This UWB signal is FCC compliant. The flat spectrum is a result of the triangular subcarrier waveform. The power spectral density of a wideband FM signal is determined by

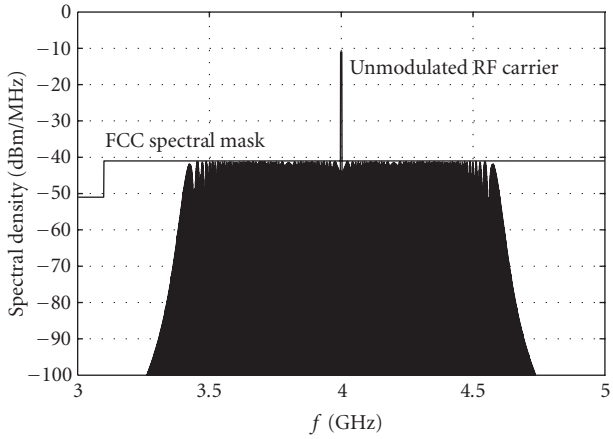

Figure 5: Spectral density S (dBm/MHz) of the unmodulated carrier at 4 GHz and the UWBFM signal obtained with $f_{\text{SUB}} = 1$ MHz and $\beta = 600$.

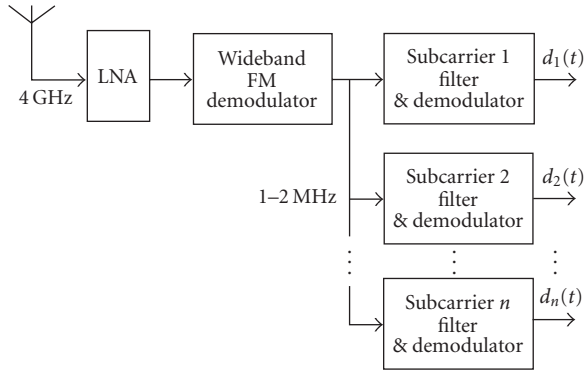

Figure 6: Block diagram of the UWBFM receiver.

and has the shape of the probability density function (pdf) of the modulating signal $m(t)$ [6].

Triangular subcarrier waveforms have a uniform pdf and therefore yield a flat RF spectrum. From a realization point of view, the triangular waveform is relatively straightforward to generate using integrated circuits.

The receiver demodulates the UWBFM signal without frequency translation. No local oscillator and no carrier synchronization are required. Figure 6 shows the block diagram of the UWBFM receiver. The receiver in its basic form comprises a wideband FM demodulator, one or several low-frequency subcarrier filtering and amplification stages, and subcarrier demodulators. One possible implementation uses a bandpass filter to filter out the wanted subcarrier signal followed by a phase-locked loop (PLL) to perform the FSK demodulation.

3. WIDEBAND FM DEMODULATOR, SNR CONVERSION

The wideband FM demodulator is implemented as a delay-line demodulator as shown in Figure 7, where $\tau = N/(4f_c)$ with $N = 1, 3, 5, \ldots$. The operation of the delay-line demodulator is that of FM-to-PM conversion in the delay line followed by a phase detector [7].

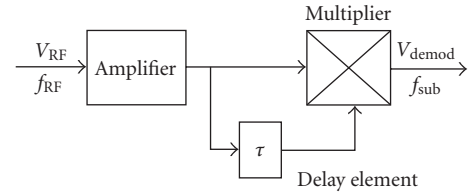

Figure 7: Delay-line FM demodulator.

We will now analyze this demodulator for a single-input signal V_1 of amplitude A_1 as given below:

$$\begin{aligned} V_1(t) &= A_1 \sin\left(\omega_{c1}t + \varphi_1(t)\right) \\ &= A_1 \sin\left(\omega_{c1}t - \beta\cos\left(\omega_m t\right)\right). \end{aligned} \tag{9}$$

The multiplier output signal V_{DEMOD} equals

$$\begin{aligned} V_{\text{DEMOD}}(t) = A_1^2 &\sin\left(\omega_{c1}t + \varphi_1(t)\right) \\ &\times \sin\left(\omega_{c1}(t-\tau) + \varphi_1(t-\tau)\right). \end{aligned} \tag{10}$$

If we ignore the high-frequency term at $2\omega_{c1}$—a component that can be easily filtered out in a practical circuit realization—the lowpass filtered output signal V_{DEMODLP} can be written as

$$V_{\text{DEMODLP}}(t) = \frac{A_1^2}{2}\cos\left(\omega_{c1}\tau + \varphi_1(t) - \varphi_1(t-\tau)\right). \tag{11}$$

By choosing the delay time τ equal to an odd multiple of a quarter period (T) for the carrier frequency f_c of the FM signal

$$\tau = N\frac{T}{4} = N\frac{\pi}{2\omega_c}, \quad N = 1, 3, 5, \ldots, \tag{12}$$

equation (11) can be rewritten as

$$V_{\text{DEMODLP}}(t) = (-1)^{((N+1)/2)}\frac{A_1^2}{2}\sin\left(\varphi_1(t) - \varphi_1(t-\tau)\right). \tag{13}$$

When the delay τ is much smaller than the period T_m of the modulating waveform of frequency f_m (i.e., requiring that $f_m \ll f_{c1}$), this can be written as

$$V_{\text{DEMODLP}}(t) = (-1)^{((N+1)/2)}\frac{A_1^2}{2}\sin\left(\tau\frac{\partial\varphi_1(t)}{\partial t}\right). \tag{14}$$

Substituting (3) and (12) in (14) yields

$$V_{\text{DEMODLP}}(t) = (-1)^{((N+1)/2)}\frac{A_1^2}{2}\sin\left(N\frac{\pi}{2}\frac{\Delta\omega}{\omega_c}\sin\left(\omega_m t\right)\right). \tag{15}$$

This corresponds to a constant times the sine of the original modulating signal $m(t)$.

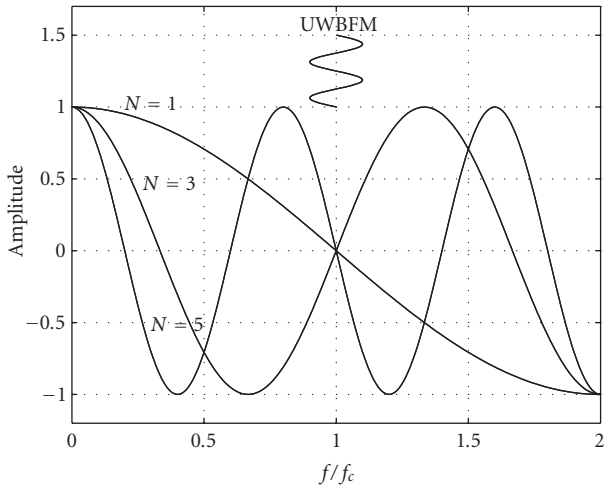

Figure 8: Normalized relation between delay-line demodulator input frequency $V_{\text{FMDEMOD}}(f)$ and output voltage for various values of N.

The demodulator output voltage as a function of the input frequency $V_{\text{FMDEMOD}}(f)$ is given by

$$V_{\text{FMDEMOD}}(f) = \frac{A_1^2}{2}\cos\left(N\frac{\pi}{2}\frac{f}{f_c}\right). \tag{16}$$

Figure 8 illustrates this relation for various values of the parameter N.

The demodulator sensitivity is proportional to N. The useful RF bandwidth B_{DEMOD} of the FM demodulator is inversely proportional to N and given by

$$B_{\text{DEMOD}} = \frac{2}{N}f_c. \tag{17}$$

The useful bandwidth is defined as the maximum frequency range over which the static demodulator transfer function is monotonic.

We define the FM demodulator overdrive O as

$$O = \frac{2\Delta f}{B_{\text{DEMOD}}} = N\frac{\Delta f}{f_c}. \tag{18}$$

Equation (15) can now be rewritten as

$$V_{\text{DEMODLP}}(t) = (-1)^{((N+1)/2)}\frac{A_1^2}{2}\sin\left(O\frac{\pi}{2}\sin(\omega_m t)\right). \tag{19}$$

An overdrive $O = 1$ corresponds to a deviation of the FM input signal equal to one half of the FM demodulator bandwidth.

It is important to note that the demodulator output signal amplitude is proportional to the square of the input signal amplitude. As a result, the dynamic range of the demodulated signal is expanded. A 20 dB variation at RF yields 40 dB after the demodulator. This strongly impacts the subcarrier filtering. A direct-conversion architecture for the subcarrier filtering and demodulation relaxes the baseband filter specifications.

Table 1: Harmonic distortion as a function of the overdrive O.

Overdrive O	HD_3 (dBc)	HD_5 (dBc)
0.05	−72	−154
0.10	−60	−130
0.20	−48	−106
0.50	−31	−74
1.00	−18	−48

Table 2: Harmonic distortion as a function of the relative frequency offset o for an overdrive $O = 0.50$.

Offset o	HD_2 (dBc)	HD_3 (dBc)
0.05	−36	−31
0.10	−30	−31
0.20	−24	−31
0.50	−7	−21

The sinusoidal transfer function of the demodulator yields odd harmonic distortion in the output signal. This distortion is a function of the overdrive O. A frequency offset in the transmitter carrier frequency f_c, with respect to the demodulator center frequency, results in even-order harmonic distortion. We define the relative offset o as

$$o = \frac{2\Delta f_C}{B_{\text{DEMOD}}}. \tag{20}$$

Numerical values can be obtained by examining the behavior of the function y:

$$y = \sin\left(o + O\frac{\pi}{2}\sin(x)\right). \tag{21}$$

Table 1 presents values for the third and fifth harmonic distortions for various values of the overdrive O and zero-frequency offset. Table 2 illustrates the effect of the frequency offset on the harmonic distortion for a fixed overdrive $O = 0.50$.

It appears that in a practical UWBFM system, multipath is a major source of distortion due to the envelope variations it introduces. As can be seen from (15), the delay-line demodulator is sensitive to both AM and FM.

Consider the AM input signal $V_{\text{AM}}(t)$ of frequency f_c and time dependent amplitude $A(t)$ given by

$$V_{\text{AM}}(t) = A(t)\sin(\omega_c t). \tag{22}$$

The multiplier output signal V_{DEMOD} can be written as

$$V_{\text{DEMOD}}(t) = A(t)A(t-\tau)\sin(\omega_c t)\sin(\omega_c(t-\tau)). \tag{23}$$

If we ignore the high-frequency term at $2\omega_c$, the lowpass filtered output signal V_{DEMODLP} can be written as

$$\begin{aligned} V_{\text{DEMODLP}}(t) &= \frac{1}{2}A(t)A(t-\tau)\cos(\omega_c\tau) \\ &\approx \frac{1}{2}A^2(t)\cos(\omega_c\tau). \end{aligned} \tag{24}$$

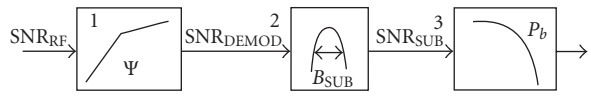

Figure 9: UWBFM receiver block diagram for determining the output probability of error P_b.

The approximation is valid for amplitude variations whose bandwidth is much smaller than $1/\tau$. An amplitude-modulated signal with sinusoidal modulation at modulation frequency f_m has a time-varying envelope $A(t)$ given by

$$A(t) = A_1(1 + m\cos(\omega_m t)). \tag{25}$$

The lowpass filtered demodulated signal V_{DEMODLP} is equal to

$$V_{\text{DEMODLP}}(t) = A_1^2\left[1 + \frac{m^2}{2} + 2m\cos(\omega_m t) + \frac{m^2}{2}\cos(2\omega_m t)\right]\cos(\omega_c \tau) \tag{26}$$

which for low-modulation depth m can be approximated by

$$V_{\text{DEMODLP}}(t) \approx A_1^2[1 + 2m\cos(\omega_m t)]\cos(\omega_c t). \tag{27}$$

This implies that the AM sensitivity equals zero at the operating points chosen for FM demodulation as given by (12) and has its maximum values in between, where the term $\cos(\omega_c\tau)$ has its extreme values. As a result, the delay-line demodulator provides strong AM rejection for narrowband signals centered on those operating points. This fact can be exploited to lower the demodulator output voltage for out-of-band interfering signals with a strong AM component (like OFDM WLAN signals at 5.25 GHz).

4. BER PERFORMANCE WITH AWGN

This section illustrates how the double FM system performs under AWGN conditions. Figure 9 shows a receiver block diagram useful for calculating the probability of error P_b of the digital output signal.

It consists of a cascade of the following blocks:

(1) wideband FM demodulator;
(2) subcarrier filter;
(3) subcarrier demodulator.

The wideband FM demodulator acts as an SNR converter. The SNR at the wideband demodulator output is a nonlinear function of the input SNR:

$$\text{SNR}_{\text{DEMOD}} = \Psi(\text{SNR}_{\text{RF}}). \tag{28}$$

Next, the bandwidth of the demodulated signal B_{DEMOD} is limited to the bandwidth B_{SUB} of the FSK subcarrier signal in the subcarrier bandpass filter. The subcarrier SNR (SNR_{SUB}) is given by

$$\text{SNR}_{\text{SUB}} = \frac{B_{\text{DEMOD}}}{B_{\text{SUB}}}\,\text{SNR}_{\text{DEMOD}}. \tag{29}$$

This SNR_{SUB} determines the probability of error at the subcarrier demodulator output. Assuming binary FSK with coherent detection and a modulation index $\beta_{\text{SUB}} = 1$ for the subcarrier modulation scheme, the probability of error P_b equals [8]

$$P_b = \frac{1}{2}\,\text{erfc}\sqrt{\frac{\text{SNR}_{\text{SUB}}}{2}}. \tag{30}$$

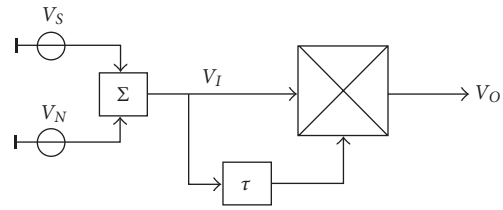

Figure 10: FM demodulator model for calculating the SNR transfer Ψ.

The calculation of the SNR transfer function Ψ of the FM demodulator is based upon the model presented in Figure 10.

The exact mathematical calculation is rather tedious [9]; it appears that the noise conversion depends on the offset o. The following intuitive calculation assumes a frequency offset $o = 0$ and autocorrelation of the noise $R_N(\tau) = 1$ for values of the delay τ according to (12). Although a rather coarse approximation, it yields results that correspond well to measurements made on a hardware prototype of the wideband demodulator.

The FM demodulator's input voltage V_I consists of the sum of signal voltage V_S and noise voltage V_N. By definition, the signal power S and noise power N are equal to $S = V_S^2$ and $N = V_N^2$. The bandwidth of both signals is $B_{\text{RF}} = 2(\beta + 1)f_{\text{SUB}}$.

The FM demodulator's output voltage V_O equals

$$\begin{aligned} V_O = V_I^2 &= (V_S + V_N)^2 \\ &= V_S^2 + V_N^2 + 2V_S V_N \\ &= S + N + 2\sqrt{S}\sqrt{N} \\ &= V_{SO} + V_{N1O} + V_{N2O}. \end{aligned} \tag{31}$$

The output voltage V_O is the sum of one signal term V_{SO} and two independent noise terms V_{N1O} and V_{N2O}. The output signal power S_O and the output noise power N_O are as follows:

$$\begin{aligned} S_O &= S^2, \\ N_O &= N^2 + 4SN. \end{aligned} \tag{32}$$

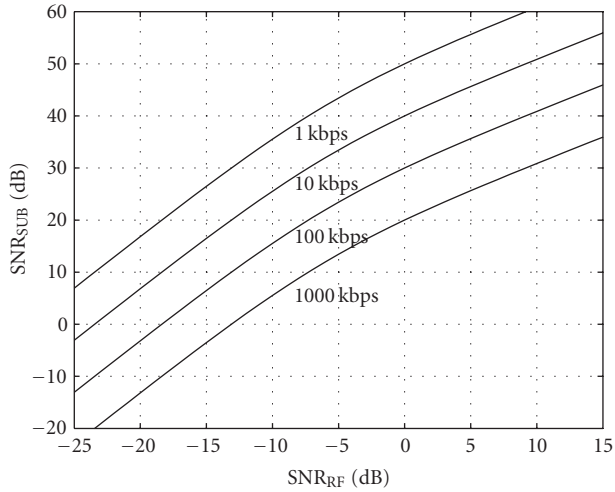

FIGURE 11: SNR conversion at various bit rates with AWGN for R = 1–1000 kbps, B_{RF} = 1 GHz, and β_{sub} = 1.

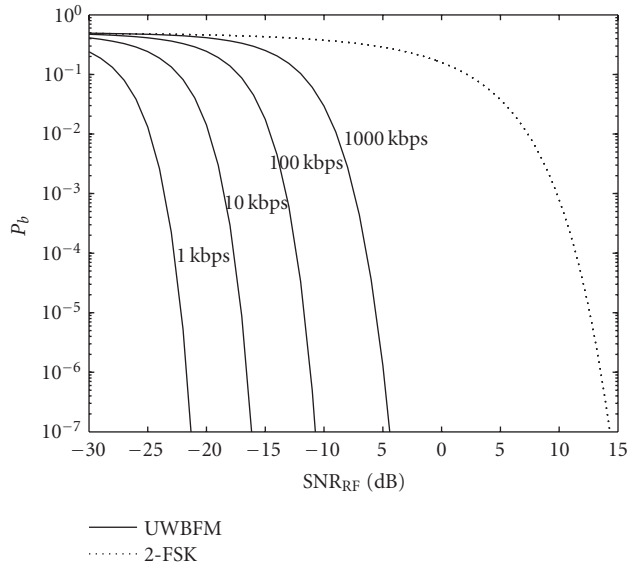

FIGURE 12: Probability of error P_b for various bit rates for an FSK and a 1 GHz bandwidth UWBFM system (R = 1–1000 kbps, B_{RF} = 1 GHz, and β_{sub} = 1).

The output SNR is then given by

$$\frac{S_O}{N_O} = \Psi\left(\frac{S}{N}\right) = \frac{S^2}{N^2 + 4SN} = \left(\frac{S}{N}\right)^2 \left(\frac{1}{1 + 4(S/N)}\right). \quad (33)$$

This expression can be approximated by

$$\frac{S_O}{N_O} = \Psi\left(\frac{S}{N}\right) \approx \left(\frac{S}{N}\right)^2 \quad \text{for } \frac{S}{N} \ll 1, \quad (34)$$

$$\frac{S_O}{N_O} = \Psi\left(\frac{S}{N}\right) \approx \frac{1}{4}\frac{S}{N} \quad \text{for } \frac{S}{N} \gg 1. \quad (35)$$

Equation (34) corresponds to the operation below threshold, while (35) corresponds to the operation above threshold. Assuming a flat spectrum for the noise terms V_{N1O} (noise × noise) and V_{N2O} (noise × noise) of B_{RF}, and referring to Figure 9, we can now calculate the SNR_{SUB} at the input of the FSK demodulator as follows:

$$SNR_{SUB} = \frac{B_{RF}}{B_{SUB}} \frac{S_{DEMOD}}{N_{DEMOD}} = \frac{B_{RF}}{B_{SUB}} SNR_{RF}^2 \left(\frac{1}{1 + 4\,SNR_{RF}}\right). \quad (36)$$

Figures 11 and 12 illustrate results for data rates R from 1 to 1000 kbps. The subcarrier modulation index β_{SUB} is constant and equal to 1, resulting in a subcarrier bandwidth $B_{SUB} = 2R$. Figure 11 shows the SNR_{SUB} as a function of the RF SNR (SNR_{RF}). A 10-fold increase in data rate results in a 10-fold increase of the subcarrier bandwidth and gives a 10 dB shift downwards in the SNR curve of Figure 11.

Figure 12 shows the probability of error P_b as a function of the SNR_{RF} for the UWBFM system with constant 1 GHz bandwidth for various data rates. For comparison, the figure also shows the probability of error for a narrowband binary FSK system occupying an RF bandwidth B_{SUB}.

In a narrowband frequency modulation (NBFM) system, no SNR conversion occurs and therefore, the four curves coincide.

A fair comparison between UWBFM and FSK can be made for signals having equal signal power (resulting in equal energy per transmitted bit E_b) and equal receiver noise single-sided power density N_0. Figure 13 shows the results of such a comparison; the probability of error P_b is shown as a function of E_b/N_0. It can be concluded that for LDRs, there is a considerable penalty in the receiver performance.

The reason is that for LDRs and error probability values higher than 1E-6, the wideband FM demodulator is always operating below threshold. At MDRs, the situation gets better and the difference between FSK and UWBFM lowers to 11 dB at a data rate of 1000 kbps.

At even higher data rates, the difference remains constant, since now the wideband FM demodulator operates above threshold and the SNR_{SUB} increases linearly with the SNR_{RF}. The performance degradation is also a function of the subcarrier modulation index. A smaller value of β_{SUB} lowers the performance penalty. Figure 14 illustrates this phenomenon for a fixed data rate of 1000 kbps and subcarrier modulation index values of 0.5, 1, 2, 4, and 8.

What does this imply for the link budget of a typical UWBFM communications system operating at 4 GHz with a bandwidth of 1 GHz, and data rate R, subcarrier modulation index β_{sub} = 1, at an error probability P_b of 1E-6?

The answer is relatively straightforward in terms of pathloss, defined as the difference (dB) between the transmitted power P_{TX} and the received power P_{RX} as

$$PL_{dB} = 10\log_{10}\left(\frac{P_{TX}}{P_{RX}}\right). \quad (37)$$

Substituting $B_{SUB} = 2R$ into (36), it is straightforward to calculate the required SNR_{RF} and obtain the SNR_{SUB} of 14 dB required to obtain P_b = 1E-6. One finds values for SNR_{RF} between −22 dB(R = 1 kbps) and −5 dB(1000 kbps).

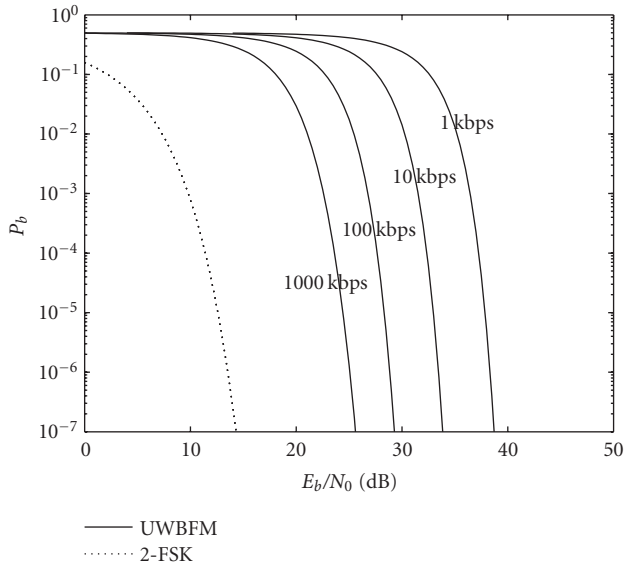

Figure 13: Probability of error P_b comparison for UWBFM and FSK (R = 1–1000 kbps, B_{RF} = 1 GHz, and β_{sub} = 1).

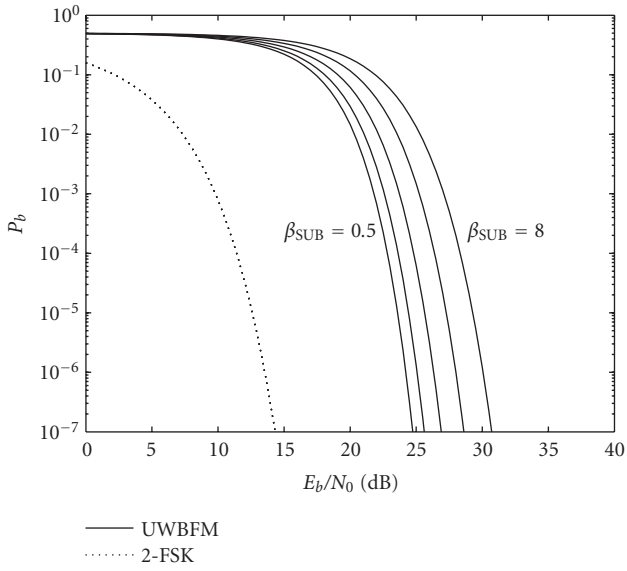

Figure 14: Probability of error P_b comparison for UWBFM and FSK with β_{SUB} values of 0.5, 1, 2, 4, and 8 (R = 1000 kbps).

The equivalent receiver's input noise power P_{NRX} for an RF bandwidth B_{RF} and a receiver noise figure NF is equal to

$$P_{NRX} = kT\,\mathrm{NF}\,B_{RF}. \tag{38}$$

Expressed in dBm and with the noise figure expressed in dB, (38) yields

$$P_{NRX,dBm} = 10\log_{10}(k\mathrm{TB}_{RF}) + \mathrm{NF}_{dB} + 30 \quad (\mathrm{dBm}). \tag{39}$$

Assuming a receiver noise figure NF of 3 (5 dB), this yields an equivalent noise power $P_{NRX} = -79$ dBm at the receiver input. Figure 15 shows the received power as a function of the distance under free-space propagation conditions, assuming isotropic antennas with an efficiency of 100%. Transmit power equals −11 dBm, the maximum power allowed for a UWB system with 1 GHz bandwidth.

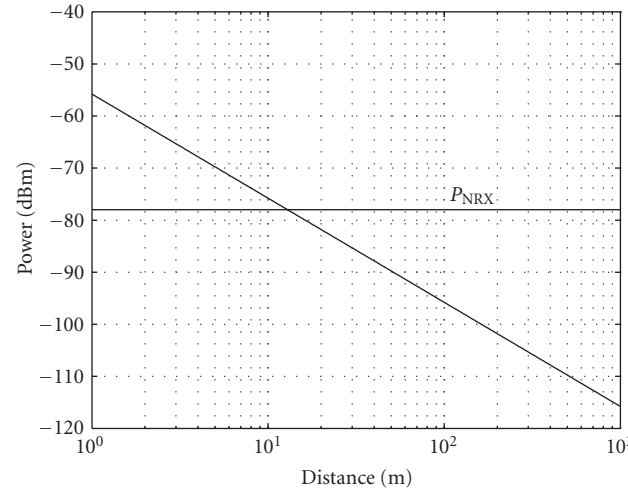

Figure 15: Received signal P_{RX} (dBm) as a function of distance under free-space propagation conditions at 4 GHz and equivalent input receiver noise power.

Table 3: Required SNR_{RF}, allowable pathloss, and equivalent free-space range to obtain P_b = 1E-6 for various data rates assuming AWGN conditions, and β_{SUB} = 1.

Data rate R (kbps)	SNR_{RF} (dB)	PL (dB)	d_{FS} (m)
1	−22	90	183
10	−17	85	106
100	−11	79	52
1000	−5	73	25

The pathloss can be written as

$$\mathrm{PL}_{dB} = 10\log_{10}\left(\frac{P_{TX}}{\mathrm{SNR}_{RF}\,P_{NRX}}\right). \tag{40}$$

Under free-space propagation conditions, using a subcarrier deviation β_{sub} = 1, and a bit rate varying between 1 and 1000 kbps, a pathloss (at the center frequency f_c) between 90 and 73 dB can be dealt with, as shown in Table 3.

Table 3 also shows the equivalent range d_{FS} that can be covered under free-space propagation conditions. These figures indicate a good link margin for LDR and MDR WPAN applications.

These results reveal that there is room for LDR and MDR UWBFM systems. Their performance is degraded by 10–15 dB with respect to narrowband FM systems, however in return, the UWBFM provides robustness against interference and multipath that is not available in narrowband FSK systems.

5. MULTIUSER UWBFM SYSTEMS AND ROBUSTNESS AGAINST NARROWBAND INTERFERENCE

In a traditional FM receiver, a limiting device removing AM components precedes an FM demodulator. Simultaneous demodulation of multiple FM signals is not possible in such a system. Usually, simultaneous demodulation is considered undesirable. In an FM broadcast radio, it clearly makes no sense to demodulate all of the FM broadcast stations simultaneously.

In a WPAN, a limited number of users may need to communicate together at the same time. This can be accomplished using time-division multiple-access (TDMA) techniques as in the GSM system, for example, which requires synchronization between the users. In a WPAN application, it would be much more elegant if little or no coordination between the users is required.

In UWBFM, an FDMA technique is used assigning different subcarrier frequencies to different users. Using an FM demodulator without hardlimiting, allows for simultaneous demodulation of multiple FM signals. We will now show mathematically that this is possible. We assume that the demodulator input signal is the sum of two UWBFM signals V_1 and V_2 of amplitudes A_1 and A_2, phases φ_1 and φ_2, carrier frequencies f_{c1} and f_{c2}, and message signals m_1 and m_2 having a subcarrier frequency of f_{m1} and f_{m2}:

$$\begin{aligned} V(t) &= V_1(t) + V_2(t) \\ &= A_1 \sin\left(\omega_{c1}t + \varphi_1(t)\right) + A_2 \sin\left(\omega_{c2}t + \varphi_2(t)\right). \end{aligned} \tag{41}$$

The demodulator output signal V_{DEMOD} now equals

$$\begin{aligned} V_{\mathrm{DEMOD}}(t) &= \{V_1(t) + V_2(t)\}\{V_1(t-\tau) + V_2(t-\tau)\} \\ &= V_1(t)V_1(t-\tau) + V_2(t)V_2(t-\tau) \\ &\quad + V_1(t)V_2(t-\tau) + V_1(t-\tau)V_2(t). \end{aligned} \tag{42}$$

The first two terms of (42) represent the useful signal $U(t)$:

$$U(t) = V_1(t)V_1(t-\tau) + V_2(t)V_2(t-\tau), \tag{43}$$

which after lowpass filtering yields the sum of the two modulating signals m_1 and m_2.

The last two terms of (42) constitute the residue $W(t)$:

$$W(t) = V_1(t)V_2(t-\tau) + V_2(t)V_1(t-\tau). \tag{44}$$

This residue may corrupt the useful signal $U(t)$.

We will now investigate the low-frequency terms of the residue $W(t)$ (obtained by a lowpass filter at half the carrier frequency f_c) in more detail. Writing out the individual low-frequency terms yields

$$\begin{aligned} W_{\mathrm{LF}}(t) &= \frac{A_1A_2}{2}\cos\left\{(\omega_{c1}-\omega_{c2})t+\omega_{c2}\tau+\varphi_1(t)-\varphi_2(t-\tau)\right\} \\ &\quad + \frac{A_1A_2}{2}\cos\left\{(\omega_{c2}-\omega_{c1})t+\omega_{c1}\tau+\varphi_2(t)-\varphi_1(t-\tau)\right\}. \end{aligned} \tag{45}$$

These two terms represent two FM signals centered at frequency $(\omega_{c1} - \omega_{c2})$ modulated by $(m_1(t) - m_2(t))$ which is the difference of the modulating signals. In other words, the residue terms are the result of asynchronous down-conversion of signals V_1 and V_2 by each other, resulting in no demodulation. The spectrum of this residue is spread over a bandwidth of $2(\Delta f_1 + \Delta f_2)$.

Figure 16 illustrates the resulting signals for the simultaneous demodulation of the two UWBFM signals of equal amplitude and carrier frequency as shown in Table 4. The two UWBFM spectra are completely overlapping. The FM demodulator is a delay-line demodulator with $N = 3$ and $f_c = 4\,\mathrm{GHz}$. Its useful bandwidth B_{DEMOD} is 2.67 GHz.

Figure 16a shows the spectrum of the RF signal $V_1 + V_2$ at the delay-line demodulator input. The two components in the demodulator output signal, that is, the useful signal $U_{\mathrm{LF}}(t)$ and the residue $W_{\mathrm{LF}}(t)$, are shown in Figure 16c. The instantaneous frequency of the residue is proportional to the difference of the two modulating signals m_1 and m_2 as shown in Figure 16b. The envelope of the residue is proportional to the sum of the two modulating signals m_1 and m_2.

Figure 17a shows the spectrum of the useful part $U_{\mathrm{LF}}(f)$ with peaks at the subcarrier frequencies and their third harmonics. Figure 17b shows the spectrum of the residue $W_{\mathrm{LF}}(f)$. Only a small part of the residue power falls within the subcarrier bandwidth.

It can be seen that the residue is spread across a bandwidth of $2(\Delta f_1 + \Delta f_2) = B_{\mathrm{RF}} = 1200\,\mathrm{MHz}$. Defining signal V_1 as the wanted signal and signal V_2 as the interference, the RF signal-to-interference ratio $\mathrm{SIR}_{\mathrm{RF}}$ is as follows:

$$\mathrm{SIR}_{\mathrm{RF}} = 20\log_{10}\left(\frac{A_1}{A_2}\right) \quad (\mathrm{dB}). \tag{46}$$

For the case where $A_1 = A_2(\mathrm{SIR}_{\mathrm{RF}} = 0\,\mathrm{dB})$, the total residue power (between 0 and B_{RF}) is equal to the signal power of one demodulated subcarrier signal.

Making the approximation that the spectrum of the residue is flat over its bandwidth, the subcarrier signal-to-interference ratio $\mathrm{SIR}_{\mathrm{SUB}}$ in the subcarrier filter bandwidth B_{SUB}, can be approximated as

$$\mathrm{SIR}_{\mathrm{SUB}} \approx \mathrm{SIR}_{\mathrm{RF}} - 10\log_{10}\left(\frac{B_{\mathrm{RF}}}{B_{\mathrm{SUB}}}\right) \quad (\mathrm{dB}). \tag{47}$$

Consider the case where $B_{\mathrm{RF}} = 1200\,\mathrm{MHz}$ and $B_{\mathrm{SUB}} = 1\,\mathrm{MHz}$; this yields $\mathrm{SIR}_{\mathrm{SUB}} = \mathrm{SIR}_{\mathrm{RF}} - 31\,\mathrm{dB}$, which is sufficient for demodulation of the subcarrier with an error probability $P_b = 1\mathrm{E}\text{-}6$, down to an $\mathrm{SIR}_{\mathrm{RF}}$ as low as $-17\,\mathrm{dB}$.

For the more general case, where the demodulator input equals the sum of N input signals $\{V_1(t), V_2(t), \ldots, V_N(t)\}$, the output signal of the wideband demodulator will comprise (according to (42)) N^2 terms: N terms of the form $V_i(t)V_i(t-\tau)$ $(i = 1, 2, \ldots, N)$ for the useful signal U, and $N(N-1)$ terms of the form $V_i(t)V_j(t-\tau)$ $(i = 1, 2, \ldots, N;\ j = 1, 2, \ldots, N,\ j \neq i)$ for the residue W. Clearly, the residue power increases with the number of users. The subcarrier SIR will decrease due to this multiple-access interference. Like in a direct-sequence CDMA system, the multiple-access interference will limit the number of users.

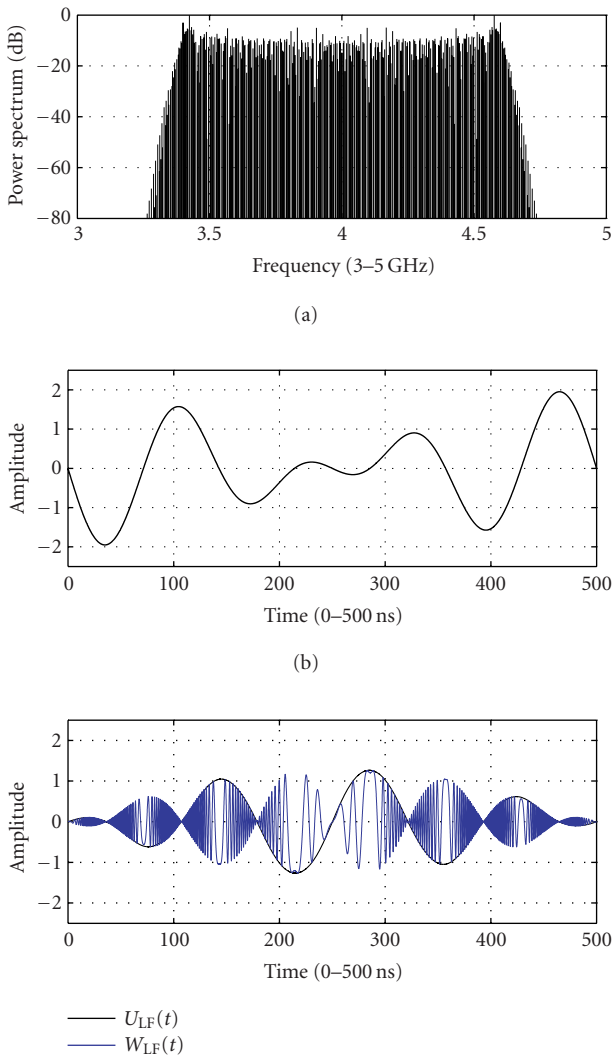

Figure 16: (a) Spectrum of the RF input signal V_1+V_2 ($S(V_1+V_2)$), (b) difference of modulating signals m_1 and m_2 ($m_1(t)-m_2(t)$), and (c) useful signal U_{LF} and residue W_{LF}.

The case of a narrowband or CW interferer is like a second user with little or no modulation. Figures 18 and 19 illustrate the case of a UWB signal with a subcarrier frequency of 20 MHz, bit rate of 2 Mbps, deviation $\Delta f = 600$ MHz, and a 20 dB stronger CW interferer. The UWB signal and interference are characterized by the parameters shown in Table 5. The high value for the subcarrier frequency and bit rate were chosen to reduce the simulation time of this SPICE simulation. The circuit is simulated over an interval of 8 microseconds and the maximum value of the time step used by SPICE equals 20 picoseconds.

Figure 18 shows the spectra of the input and output signals V_{RF} and $V_{DEMODLP}$ of the wideband demodulator.

Figure 19a shows the spectrum of the filtered subcarrier signal prior to FM demodulation. Figure 19b shows the

Table 4: Parameters of the two UWBFM signals.

UWBFM signal	1	2
RF center frequency	4 GHz	4 GHz
RF voltage	1 V	1 V
Subcarrier frequency	6 MHz	8 MHz
Subcarrier deviation	600 MHz	600 MHz

transmitted and received message signals m and m_{RX}. It can be appreciated that the UWBFM system can easily cope with the CW interferer.

The robustness to more realistic interfering signals, like inband UWB, multiband OFDM signals, and out-of-band WLAN signals will be addressed in future research.

6. MULTIPATH PERFORMANCE OF UWBFM

As mentioned in Section 3, multipath is a major source of AM components. The UWBFM signal is inherently scanning the frequency-dependent transfer function $H(f)$ of the channel. We will first illustrate this for a single-reflection channel described by the 2-path model [10] with transfer function

$$H_2(f) = 1 + a_2 e^{j\alpha_2} e^{-j2\pi f \tau_2}. \tag{48}$$

The magnitude of this transfer function equals

$$|H_2(f)| = \sqrt{1 + a_2^2 + 2a_2 \cos(2\pi f \tau_2 - \alpha_2)}. \tag{49}$$

Figure 20 shows the magnitude of this transfer function for parameter values $a_2 = 0.4$, $\alpha_2 = 0$, and $\tau_2 = 1312.5$ picoseconds. The UWBFM signal is centered at 4 GHz and has a deviation $\Delta f = 600$ MHz and a sinusoidal subcarrier signal $m(t)$ of frequency $f_m = 1$ MHz. The instantaneous frequency of this UWB signal is also sinusoidal with time and varies between 3.4 and 4.6 GHz.

The UWB signal is scanning the frequency-dependent channel transfer function $H(f)$ with the rhythm of the modulating signal $m(t)$. The amplitude $A(t)$ of the received UWB signal $V_{RX}(t)$ will vary accordingly. Figure 21 shows the subcarrier signal $m(t)$, the time-varying amplitude $A(t)$ of the receiver's input signal, as well as the resulting FM demodulator output voltage $V_{DEMODLP}(t)$; the latter is equal to the output voltage without multipath multiplied by $A^2(t)$.

Figure 22 shows the spectrum of the demodulated signal. The harmonics result from the time-varying amplitude of the received signal. This example clearly illustrates the presence of the second harmonic of the subcarrier (6 dB below the fundamental in this particular example).

In order to illustrate the performance of UWBFM for more complex channels, a case with an 8-path channel model with transfer function $H_8(f)$ has been simulated with

$$H_8(f) = \sum_{i=1}^{8} a_i e^{j\alpha_i} e^{-j2\pi f \tau_i}. \tag{50}$$

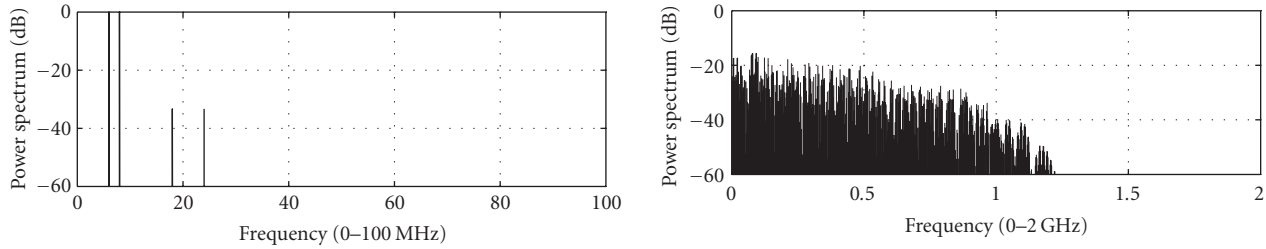

Figure 17: (a) Spectrum of the useful part $U_{\mathrm{LF}}(f)$ and (b) spectrum of the residue $W_{\mathrm{LF}}(f)$ of the demodulated signal.

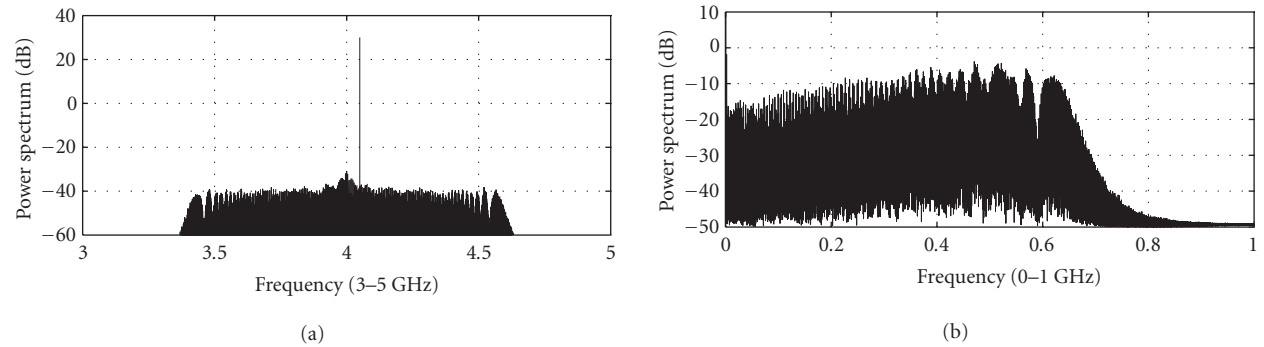

Figure 18: Spectrum of wideband demodulator input and output signals (a) $V_{\mathrm{RF}}(f)$ and (b) $V_{\mathrm{DEMODLP}}(f)$ for a 20 dB stronger CW interferer.

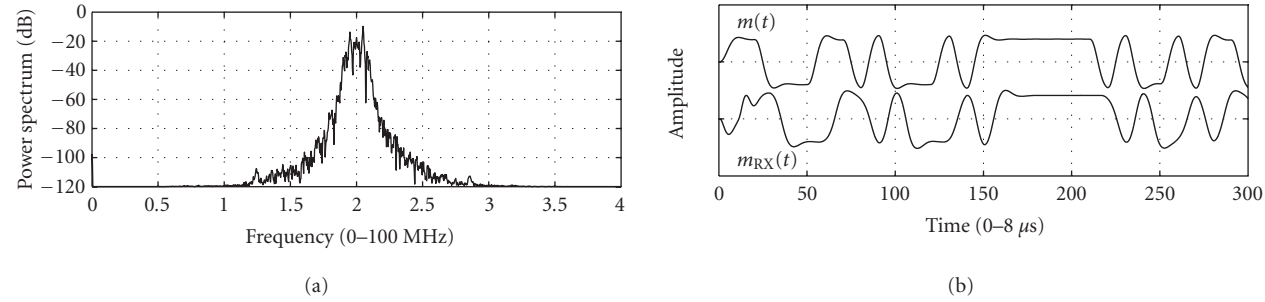

Figure 19: (a) Spectrum of the subcarrier demodulator input signal $V_{\mathrm{DEMODLP}}(f)$ and (b) transmitted message $m(t)$ and received message $m_{\mathrm{RX}}(t)$.

Table 5: Parameters of the UWBFM and CW jammer signal.

Signal	UWBFM	CW
RF center frequency	4 GHz	4 GHz
RF voltage	1 V	10 V
Subcarrier frequency	20 MHz	—
Subcarrier deviation	600 MHz	—

The coefficients $\{a_i, \alpha_i, \tau_i\}$ are given in Table 6. This model represents a short-range communications channel with one attenuated direct component plus seven delayed components.

Figure 23 shows the magnitude $|H_8(f)|$ of the frequency-domain transfer function of this 8-path channel. Figure 24 shows the subcarrier signal $m(t)$, the time-varying amplitude $A(t)$ of the receiver's input signal, as well as the resulting FM demodulator output voltage $V_{\mathrm{DEMODLP}}(t)$ for this more complex channel.

Clearly, $A(t)$ is changing rapidly with time. Figure 25 shows the spectrum of the demodulated signal. The second harmonic of the subcarrier is still present and the number of harmonics has significantly increased.

Since the fundamental of the subcarrier frequency is always present, the demodulation of this signal is not affected. The bandpass filtering already present to implement

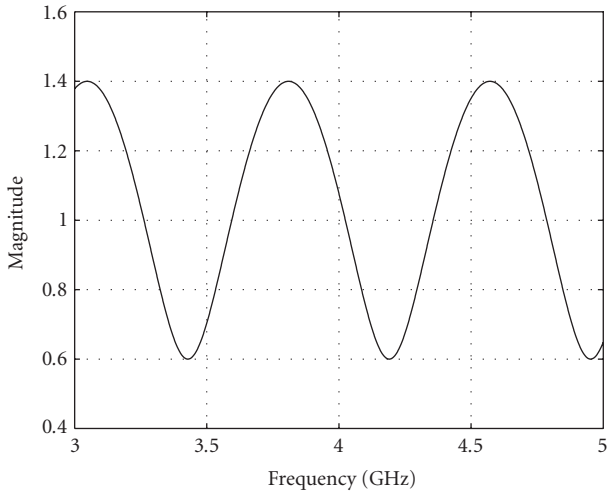

Figure 20: Magnitude $|H_2(f)|$ of the channel transfer function.

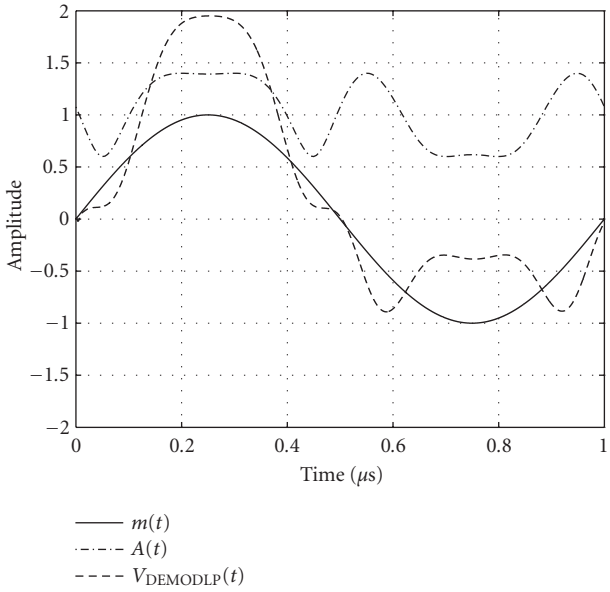

Figure 21: Original modulating signal $m(t)$, time-varying amplitude $A(t)$, and demodulator output signal $V_{\text{DEMODLP}}(t)$ for the 2-path channel.

the subcarrier filtering will remove the subcarrier harmonics prior to demodulation. UWBFM is therefore robust to multipath.

However, the second and higher harmonic components will camouflage any useful signal whose subcarrier is at their frequency. Figure 26 illustrates what may happen for the LDR-MDR UWBFM system using subcarrier frequencies between 1 and 2 MHz as shown in Figure 4. The second harmonic components fill up the frequency range between 2 and 4 MHz.

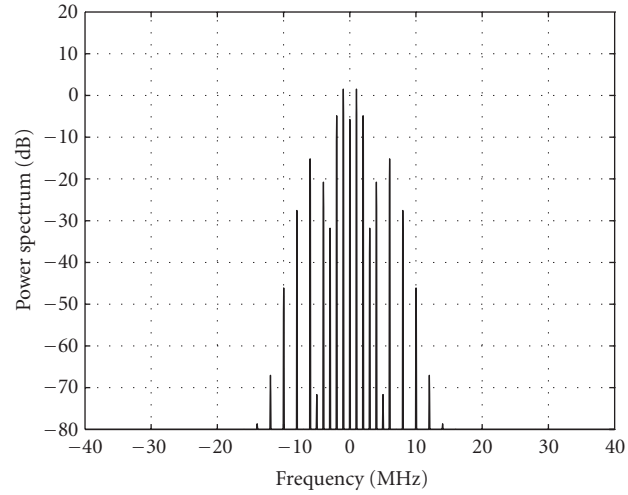

Figure 22: Spectrum of the demodulator output signal $S(V_{\text{DEMODLP}})$ in the case of a 2-path channel with $a_2 = 0.4$.

Table 6: Coefficients of the 8-path channel model.

a_i	α_i	τ_i (ns)
0.30	0	0
0.11	0	2.5
0.21	0	3.5
0.33	0	4.0
0.50	0	4.688
0.37	0	5
0.22	0	5.5
0.10	0	6.5

If no form of equalization is used, the useful subcarrier frequency range is limited to a single octave. Equalization is the subject of further investigations.

7. CONCLUSION

A novel frequency-domain UWB technology has been presented. UWBFM uses double FM: low-modulation index digital FSK followed by high-modulation index analog FM to create a constant-envelope UWB signal whose spectral density is lowered by a factor equal to the modulation index β. The UWBFM center frequency and bandwidth can be easily controlled and the spectral roll-off is steep.

The performance degradation compared to NBFM systems is between 10 and 15 dB in terms of probability of error performance and depends on the subcarrier modulation index. Despite this degradation, a 1 GHz bandwidth UWB communications system operating at a center frequency of 4 GHz has a range of 25 m under free-space

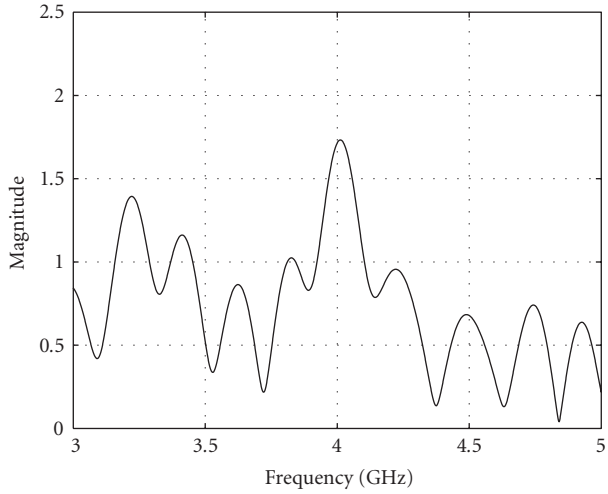

Figure 23: Magnitude $|H_8(f)|$ of the channel transfer function.

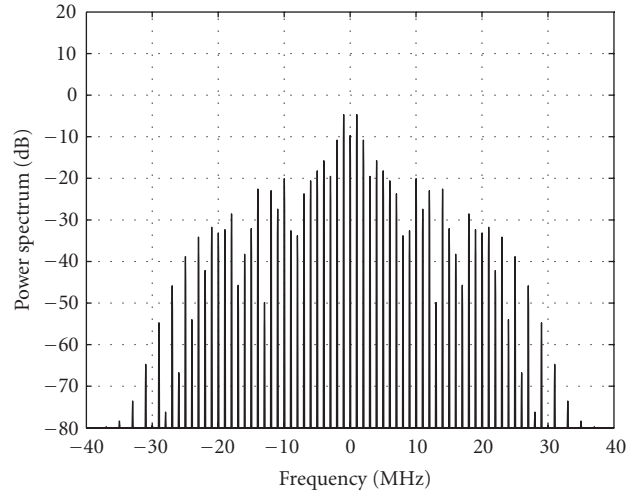

Figure 25: The spectrum of the demodulator output signal $S(V_{\text{DEMODLP}})$ for the 8-path channel.

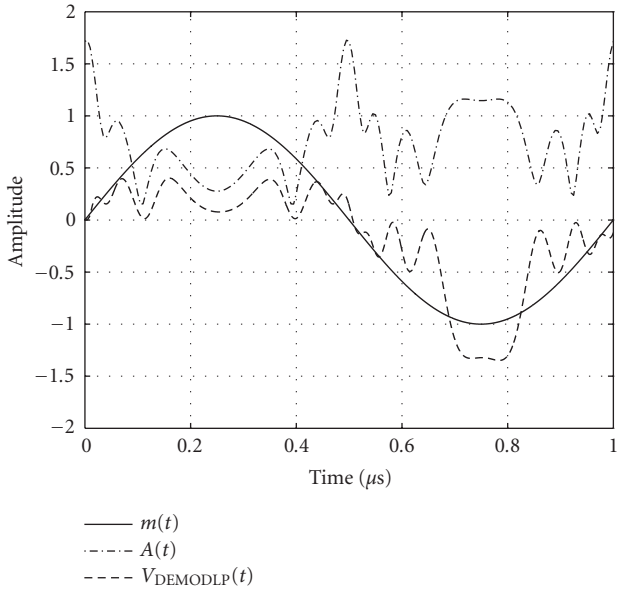

Figure 24: Original modulating signal $m(t)$, time-varying amplitude $A(t)$, and resulting demodulator output signal $V_{\text{DEMODLP}}(t)$ for the 8-path channel.

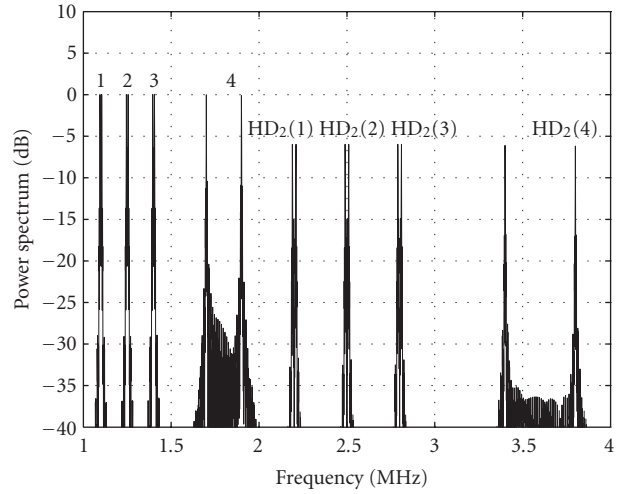

Figure 26: Effect of second harmonic distortion on the spectrum $S(f)$ after the wideband FM demodulator for a 1–2 MHz subcarrier system.

propagation conditions when operating at 1 Mbps and 100 m at 10 kbps, yielding a good link margin for LDR and MDR WPAN applications. Moreover, UWBFM provides robustness against interference and multipath, especially for low bit rates, that is not available in NBFM systems.

Characterization, modeling, and subsequent mitigation of in-band interference from other UWB systems like impulse radio and multiband OFDM, as well as strong out-of-band signals like WLANs will be addressed in future research.

Multiple subcarriers can accommodate multiple users. Simultaneous demodulation of the various UWBFM signals is achieved in a wideband FM demodulator that is not preceded by any limiting device. However, due to the squaring action of the demodulator, the dynamic range of the demodulated signal expands, requiring steep subcarrier filtering. The number of users is also limited by multiple-access interference, which is a subject for future research.

Multipath introduces envelope variations in the amplitude of the received signal that result in harmonic distortion of the demodulated UWBFM signal. Without equalization, the useful subcarrier range is limited to one octave. Equalization techniques will also be addressed in future research.

ACKNOWLEDGMENTS

This work was partially carried out in the context of the Sixth Framework IST Project 507102, "MAGNET" (My Personal Adaptive Global NET). The IST Program is partially funded by the EC. The authors would like to thank the EC for their support.

REFERENCES

[1] Federal Communication Commission (FCC), "Revision of part 15 of the commission's rules regarding ultra wideband transmission systems," First Report and Order, ET Docket 98–153, FCC 02–48; Adopted:February 2002; Released:April 2002.

[2] M. Z. Win and R. A. Scholtz, "Impulse radio: how it works," *IEEE Commun. Lett.*, vol. 2, no. 2, pp. 36–38, 1998.

[3] A. Batra, J. Balakrishnan, and A. Dabak et al., "Multi-band OFDM Physical Layer Proposal for IEEE 802.15 Task Group 3a," MultiBand OFDM Alliance SIG, September 2004.

[4] J. Farserotu, A. Hutter, F. Platbrood, J. Ayadi, J. Gerrits, and A. Pollini, "UWB transmission and MIMO antenna systems for nomadic users and mobile PANs," *Wireless Personal Communications*, vol. 22, no. 2, pp. 297–317, 2002.

[5] J. Gerrits and J. Farserotu, "Ultra wideband FM: A straightforward frequency domain approach," in *Proc. 33rd European Microwave Conference (EuMC '03)*, vol. 2, pp. 853–856, Munich, Germany, October 2003.

[6] H. Taub and D. Schilling, *Principles of Communication Systems*, McGraw-Hill, New York, NY, USA, 1971.

[7] M. H. L. Kouwenhoven, *High-Performance Frequency-Demodulation Systems*, Delft University Press, Delft, the Netherlands, 1998.

[8] J. G. Proakis, *Digital Communications*, McGraw-Hill, New York, NY, USA, 3rd edition, 1995.

[9] M. H. L. Kouwenhoven, "An analysis of the quadrature and math demodulator in the presence of noise," Internal Rep., Electronics Research Laboratory, Delft University of Technology, Delft, the Netherlands, November 1995.

[10] R. Vaughan and J. B. Andersen, *Channels, Propagation and Antennas for Mobile Communications*, the Institution of Electrical Engineers, London, UK, 2003.

John F. M. Gerrits was born in Leiden, The Netherlands. He received the M.S.E.E. degree from Delft University of Technology, The Netherlands, in 1987. His final thesis was on the design of integrated high-performance harmonic oscillator circuits. In 1988, he joined the Philips T&M Division in Enschede, The Netherlands, where he designed integrated oscillator and data-acquisition systems for oscilloscope applications. In 1991, he joined CSEM, where he has been involved in both system and circuit design of a single-chip low-power VHF radio receiver for hearing aid applications and of a single-chip UHF transceiver for ISM applications. His current work involves system and circuit design of UWB radio systems, RF and EM simulation techniques, and measurement methodology. He has recently started a Ph.D. on the fundamental aspects and practical realizations of UWBFM at Delft University of Technology. He is an Editor and coauthor of the book *Low-Power Design Techniques and CAD Tools for Analog and RF Integrated Circuits,* published by Kluwer in 2001. He holds 3 European and 1 US patents.

Michiel H. L. Kouwenhoven was born in Delft, The Netherlands, on July 8, 1971. He received the M.S. degree in electrical engineering from Delft University of Technology in 1993, and the Ph.D. degree from the same university in 1998. From 1997 until 2000, he was an Assistant Professor at the Electronics Research Laboratory, Delft University of Technology, were he worked on various subjects including design methodologies for electronic circuits, noise in nonlinear circuits, RF oscillator design, and demodulators. In 2000, he joined the Delft Design Centre, National Semiconductor Corporation, were he is now responsible for the design of RF power detectors, and power control devices. From 1999 until 2001, he served as an Associate Editor for the IEEE Transactions on Circuits and Systems-II. Dr. Kouwenhoven received the 1997 Veder Award from the Dutch Foundation for Radio Science (Stichting Verder) for his Ph.D. work on frequency demodulators.

Paul R. van der Meer was born in The Hague, The Netherlands, on July 24, 1970. He received the M.S. and Ph.D. degrees in electrical engineering from Delft University of Technology, Delft, The Netherlands, in 1997 and 2003, respectively. In 2001, he cofounded Mirage 3D Simulators, a company involved mainly in car driving simulation. From 2002 till now, he worked as a Postdoc. at the Electronics Research Laboratory, Delft University of Technology, in the RF field. Presently, he is cofounding Seagull Simulation Systems, a company that develops cockpit systems and parts for research, professional, and consumer flight simulators.

John R. Farserotu received the B.S.E.E. degree from the University of Maryland, College Park, Md, in 1982 and the M.S.E.E. degree in communications engineering from the George Washington University, Washington, DC, in 1986. He received his Ph.D. from the Delft University of Technology, Delft, The Netherlands, in 1998. Dr. Farserotu is currently the Head of the Wireless Communication Section in the Systems Engineering Division at CSEM, where he is responsible for leading a team of scientists and engineers working on R&D in wireless communication and implementation of advanced engineering prototypes. His research interests include mobile wireless personal area networks (WPANs), ultra-wideband (UWB) communication, robust modulation and coding, and HAP/satellite communication and networking. Dr. Farserotu has authored or coauthored over 50 publications in major journals and conferences. He is the coauthor of *IP/ATM Mobile Satellite Networks*, published by Artech House in 2001. He teaches a course on this subject at the École Polytechnique Fédérale de Lausanne (EPFL). Dr. Farserotu is currently the Vice-Chair of the HERMES Partnership, a network of major European R&D centers in the field of wireless and mobile communication bringing together over 1000 engineers and scientists.

John R. Long received the B.S. degree in electrical engineering from the University of Calgary in 1984, and the M.E. and Ph.D. degrees in electronics engineering from Carleton University in 1992 and 1996, respectively. He was employed for 10 years by Bell-Northern Research, Ottawa (now Nortel Networks), involved in the design of ASICs for Gbps fibre-optic transmission systems, and employed for 5 years at the University of Toronto. He joined the faculty at Delft University of Technology in January 2002 as a Chair of the Electronics Research Laboratory. His current research interests include low-power transceiver circuitry for highly integrated radio applications, and electronics design for high-speed data communications systems. Professor Long is currently serving on the Technical Program Committees of the International Solid-State Circuits Conference (ISSCC), the European Solid-State Circuits Conference (ESSCIRC), the IEEE Bipolar/BiCMOS Circuits and Technology Meeting (BCTM), and GAAS2004 (EuMW). He is a former Associate Editor of the IEEE Journal of Solid-State Circuits. He received the NSERC Doctoral Prize and Douglas R. Colton and Governor General's Medals for Research Excellence, and Best Paper Awards from ISSCC 2000 and IEEE-BCTM 2003.